and tends to force them apart. (Thus the differential rigidity μ can be used as an alternative to M_p in indicating whether a beam is prone or resistant to delamination.)

In Fig. 3 $p_{\max}$ is always negative except in the unlikely cases where the upper layer is thinner than 0.091 mm; this implies a resistance to delamination. Note, however, that generally thermomechanical stress in ICs arises from a temperature reduction from the curing temperature of an epoxy (usually 150°C or 175°C) to room temperature, or to a test extreme such as -65°C. Thus the case study example is in reality prone to peeling under normal usage.

An investigation was also made into the effect on μ and $p_{\max}$ of varying E_1 and E_2. This again showed that the range of possible values for μ was from $-h_1/2$ to $+h_2/2$. However, it was also found that as the moduli of elasticity increased, the maximum peeling stress $p_{\max}$ increased in proportion.

4 Conclusions

The sign of the interfacial free-edge peeling moment M_p indicates whether a bimaterial beam is prone or resistant to delamination under thermomechanical stress. This sign can be found with one simple calculation when the layer properties and the temperature change are known. The relationship between the peeling moment M_p and the differential rigidity μ of the bimaterial beam was examined. It was shown that there is a close relationship, and that the sign of the differential rigidity is also a direct indicator of the resistance—or the tendency—to peeling. Finally it was shown that upper and lower limits to the value of the differential rigidity exist; as the stiffness of one layer becomes dominant, the magnitude of the differential rigidity converges to one-half the thickness of the opposite layer.

References

[1] Moore, T. D., and Jarvis, J. L., 2003, "A Simple and Fundamental Design Rule for Resisting Delamination in Bimaterial Structures," Microelectron. Reliab., **43**(3), pp. 487–494.

[2] Timoshenko, S., 1925, "Analysis of Bi-metal Thermostats," J. Opt. Soc. Am., **11**(Sept.), pp. 233–255.

[3] Suhir, E., 1986, "Stresses in Bi-metal Thermostats," ASME J. Appl. Mech., **53**, pp. 657–660.

[4] Suhir, E., 1989, "Interfacial Stresses in Bi-metal Thermostats," ASME J. Appl. Mech., **56**, pp. 595–600.

[5] Ru, C. Q., 2002, "Interfacial Thermal Stresses in Bimaterial Beams: Modified Beam Models Revisited," ASME J. Electron. Packag., **124**, pp. 141–146.

[6] Moore, T. D., and Jarvis, J. L., 2001, "Failure Analysis and Stress Simulation in Small Multichip BGAs," IEEE Trans. Adv. Packag., **24**(2), pp. 216–223.

Triple Coordinate Transforms for Prediction of Falling Cylinder Through the Water Column

Peter C. Chu, Chenwu Fan, Ashley D. Evans, and Anthony Gilles

Naval Ocean Analysis and Prediction Laboratory, Department of Oceanography, Naval Postgraduate School, 833 Dyer Road, Monterey, CA 93943

Triple coordinate systems are introduced to predict translation and orientation of falling rigid cylinder through the water column: earth-fixed coordinate (E-coordinate), cylinder's main-axis following coordinate (M-coordinate), and hydrodynamic force following coordinate (F-coordinate). Use of the triple coordinate systems and the transforms among them leads to the simplification of the dynamical system. The body and buoyancy forces and their moments are easily calculated using the E-coordinate system. The hydrodynamic forces (such as the drag and lift forces) and their moments are easily computed using the F-coordinate. The cylinder's moments of gyration are simply represented using the M-coordinate. Data collected from a cylinder-drop experiment at the Naval Postgraduate School swimming pool in June 2001 show great potential of using the triple coordinate transforms. [DOI: 10.1115/1.1651093]

1 Introduction

Consider an axially symmetric cylinder with the centers of mass (**X**) and volume (**B**) on the main axis (Fig. 1). Let (L,d,χ) represent the cylinder's length, diameter, and the distance between the two points (**X**,**B**). The positive χ-values refer to nose-down case, i.e., the center of mass (COM) is lower than the center of volume (COV). Three coordinate systems are used to model the hydrodynamics of falling cylinder through the water column: earth-fixed coordinate (E-coordinate), cylinder's main-axis following coordinate (M-coordinate), and hydrodynamic force following coordinate (F-coordinate). All the systems are three-dimensional, orthogonal, and right-handed.

2 Triple Coordinate Systems

2.1 E-Coordinate. The E-coordinate is represented by $F_E(O,\mathbf{i},\mathbf{j},\mathbf{k})$ with the origin "O," and three axes: *x*, *y*-axes (horizontal) with the unit vectors (**i**,**j**) and z-axis (vertical) with the unit vector **k** (upward positive). The position of the cylinder is represented by the position of the COM,

$$\mathbf{X}=x\mathbf{i}+y\mathbf{j}+z\mathbf{k}, \tag{1}$$

which is translation of the cylinder. The translation velocity is given by

$$\frac{d\mathbf{X}}{dt}=\mathbf{V}, \quad \mathbf{V}=(u,v,w). \tag{2}$$

2.2 M-Coordinate. Let orientation of the cylinder's main-axis (pointing downward) is given by $\mathbf{i}_M$. The angle between $\mathbf{i}_M$ and **k** is denoted by $\psi_2+\pi/2$. Projection of the vector $\mathbf{i}_M$ onto the (x,y) plane creates angle (ψ_3) between the projection and the *x*-axis (Fig. 2). The M-coordinate is represented by $F_M(\mathbf{X},\mathbf{i}_M,\mathbf{j}_M,\mathbf{k}_M)$ with the origin "**X**," unit vectors $(\mathbf{i}_M,\mathbf{j}_M,\mathbf{k}_M)$, and coordinates (x_M,y_M,z_M). In the plane consisting of vectors $\mathbf{i}_M$ and **k** (passing through the point *M*, called the IMK plane), two new unit vectors $(\mathbf{j}_M,\mathbf{k}_M)$ are defined with $\mathbf{j}_M$ perpendicular to the IMK plane, and $\mathbf{k}_M$ perpendicular to $\mathbf{i}_M$ in the IMK plane. The unit vectors of the M-coordinate system are given by (Fig. 2)

$$\mathbf{j}_M=\mathbf{k}\times\mathbf{i}_M, \quad \mathbf{k}_M=\mathbf{i}_M\times\mathbf{j}_M. \tag{3}$$

The M-coordinate system is solely determined by orientation of the cylinder's main-axis $\mathbf{i}_M$. Let the vector **P** be represented by ${}^E\mathbf{P}$ in the E-coordinate and by ${}^M\mathbf{P}$ in the M-coordinate, and let ${}^E_M\mathbf{R}$ be the rotation matrix from the M-coordinate to the E-coordinate,

$$ {}^E_M\mathbf{R}(\psi_2,\psi_3)\equiv\begin{bmatrix} r_{11} & r_{12} & r_{13}\\ r_{21} & r_{22} & r_{23}\\ r_{31} & r_{32} & r_{33}\end{bmatrix}=\begin{bmatrix}\cos\psi_3 & -\sin\psi_3 & 0\\ \sin\psi_3 & \cos\psi_3 & 0\\ 0 & 0 & 1\end{bmatrix} \times\begin{bmatrix}\cos\psi_2 & 0 & \sin\psi_2\\ 0 & 1 & 0\\ -\sin\psi_2 & 0 & \cos\psi_2\end{bmatrix}, \tag{4}$$

Contributed by the Applied Mechanics Division of THE AMERICAN SOCIETY OF MECHANICAL ENGINEERS for publication in the ASME JOURNAL OF APPLIED MECHANICS. Manuscript received by the ASME Applied Mechanics Division, May 14, 2003; final revision, Sept. 19, 2003. Associate Editor: D. A. Siginer.

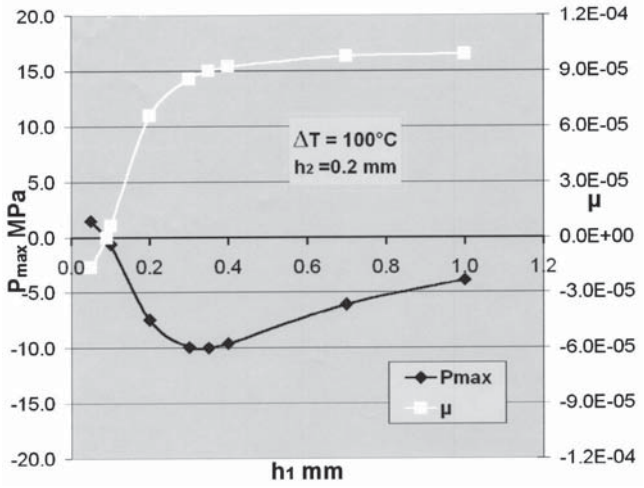

Fig. 3 Effect on μ and p_{max} of varying upper layer thickness

which represents $(\mathbf{i}_M, \mathbf{j}_M, \mathbf{k}_M)$,

$$\mathbf{i}_M = \begin{bmatrix} r_{11} \\ r_{21} \\ r_{31} \end{bmatrix}, \quad \mathbf{j}_M = \begin{bmatrix} r_{12} \\ r_{22} \\ r_{32} \end{bmatrix}, \quad \mathbf{k}_M = \begin{bmatrix} r_{13} \\ r_{23} \\ r_{33} \end{bmatrix}. \tag{5}$$

Transformation of ${}^M\mathbf{P}$ into ${}^E\mathbf{P}$ contains rotation and translation,

$${}^E\mathbf{P} = {}^E_M\mathbf{R}(\psi_2, \psi_3)\,{}^M\mathbf{P} + \mathbf{X}. \tag{6}$$

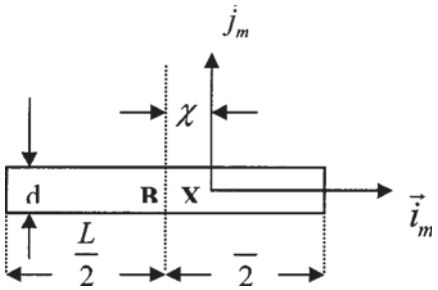

Fig. 1 M-coordinate with the COM as the origin X and $(\mathbf{i}_m, \mathbf{j}_m)$ as the two axes. Here, χ is the distance between the COV (B) and COM, (L, d) are the cylinder's length and diameter.

Let the cylinder rotate around $(\mathbf{i}_M, \mathbf{j}_M, \mathbf{k}_M)$ with angles $(\varphi_1, \varphi_2, \varphi_3)$ (Fig. 2). The angular velocity of cylinder is calculated by

$$\omega_1 = \frac{d\varphi_1}{dt}, \quad \omega_2 = \frac{d\varphi_2}{dt}, \quad \omega_3 = \frac{d\varphi_3}{dt}, \tag{7}$$

and

$$\psi_1 = \varphi_1, \quad \frac{d\psi_2}{dt} = \frac{d\varphi_2}{dt} = \omega_2, \quad \frac{d\psi_3}{dt} \neq \frac{d\varphi_3}{dt}. \tag{8}$$

If $(\omega_1, \omega_2, \omega_3)$ are given, time integration of (7) with the time interval Δt leads to

$$\Delta\varphi_1 = \omega_1 \Delta t, \quad \Delta\varphi_2 = \omega_2 \Delta t, \quad \Delta\varphi_3 = \omega_3 \Delta t. \tag{9}$$

The increments $(\Delta\psi_2, \Delta\psi_3)$ are determined by the relationship between the two rotation matrices ${}^E_M R(\psi_2 + \Delta\psi_2, \psi_3 + \Delta\psi_3)$ and ${}^E_M R(\psi_2, \psi_3)$

$$\begin{aligned} &{}^E_M R(\psi_2 + \Delta\psi_2, \psi_3 + \Delta\psi_3) \\ &\quad = {}^E_M R(\psi_2, \psi_3) \begin{bmatrix} \cos(\Delta\varphi_3) & -\sin(\Delta\varphi_3) & 0 \\ \sin(\Delta\varphi_3) & \cos(\Delta\varphi_3) & 0 \\ 0 & 0 & 1 \end{bmatrix} \\ &\quad \times \begin{bmatrix} \cos(\Delta\varphi_2) & 0 & \sin(\Delta\varphi_2) \\ 0 & 1 & 0 \\ -\sin(\Delta\varphi_2) & 0 & \cos(\Delta\varphi_2) \end{bmatrix}. \end{aligned} \tag{10}$$

2.3 F-Coordinate. The F-coordinate is represented by $F_F(\mathbf{X}, \mathbf{i}_F, \mathbf{j}_F, \mathbf{k}_F)$ with the origin $\mathbf{X}$, unit vectors $(\mathbf{i}_F, \mathbf{j}_F, \mathbf{k}_F)$, and coordinates (x_F, y_F, z_F). Let $\mathbf{V}_w$ be the fluid velocity. The water-to-cylinder velocity is represented by $\mathbf{V}_r = \mathbf{V}_w - \mathbf{V}$, that is decomposed into two parts,

$$\mathbf{V}_r = \mathbf{V}_1 + \mathbf{V}_2, \quad \mathbf{V}_1 = (\mathbf{V}_r \cdot \mathbf{i}_F)\mathbf{i}_F, \quad \mathbf{V}_2 = \mathbf{V}_r - (\mathbf{V}_r \cdot \mathbf{i}_F)\mathbf{i}_F, \tag{11}$$

where $\mathbf{V}_1$ is the component paralleling to the cylinder's main-axis (i.e., along $\mathbf{i}_M$), and $\mathbf{V}_2$ is the component perpendicular to the cylinder's main-axial direction. The unit vectors for the F-coordinate are defined by (column vectors)

$$\mathbf{i}_F = \mathbf{i}_M = \begin{bmatrix} r_{11} \\ r_{21} \\ r_{31} \end{bmatrix}, \quad \mathbf{j}_F = \mathbf{V}_2 / |\mathbf{V}_2|, \quad \mathbf{k}_F = \mathbf{i}_F \times \mathbf{j}_F. \tag{12}$$

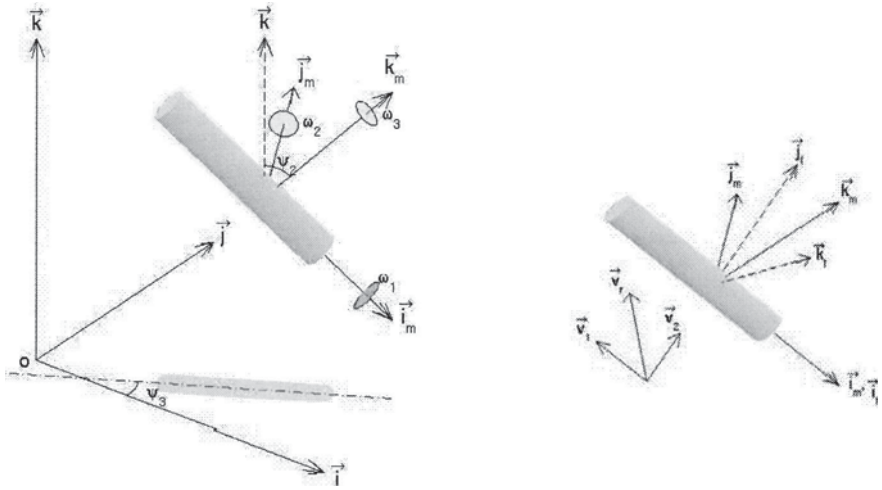

Fig. 2 Three coordinate systems

Table 1 Physical parameters of the model cylinders

Cylinder	Mass (g)	L (cm)	Volume (cm^3)	ρ_m ($g\,m^{-3}$)	J_1 ($g\,m^2$)	χ (cm)	$J_2(J_3)$ ($g\,m^2$)
	322.5	15.20	191.01	1.69	330.5	0.00	6087.9
1						0.74	5783.0
						1.48	6233.8
2	254.2	12.10	152.05	1.67	271.3	0.06	3424.6
						0.53	3206.5
						1.00	3312.6
3	215.3	9.12	114.61	1.88	235.0	0.00	1695.2
						0.29	1577.5
						0.58	1556.8

Table 2 Trajectory patterns

Trajectory Pattern	Description
Straight	Cylinder exhibited little angular change about z-axis. The attitude remained nearly parallel with z-axis ($\pm$15 deg).
Slant	Cylinder exhibited little angular change about z-axis. The attitude was 45 deg off z-axis ($\pm$15 deg).
Spiral	Cylinder experienced rotation about z-axis throughout the water column
Flip	Initial water entry point rotated at least 180 deg
Flat	Cylinder's angle with vertical near 90 deg for most of the trajectory
Seesaw	Similar to the flat pattern except that cylinder's angle with vertical would oscillate between greater (less) than 90 deg and less (greater) than 90 deg like a seesaw
Combination	Complex trajectory where cylinder exhibited several of theabove patterns

The F-coordinate system is solely determined by orientation of the cylinder's main-axis ($\mathbf{i}_M$) and the water-to-cylinder velocity. Note that the M and F-coordinate systems have one common unit vector $\mathbf{i}_M$ (orientation of the cylinder).

Let ${}^E_F\mathbf{R}$ be the rotation matrix from the F-coordinate to the E-coordinate,

$$ {}^E_F\mathbf{R}(\psi_2,\psi_3,\phi_{MF}) \equiv \begin{bmatrix} r_{11} & r'_{12} & r'_{13} \\ r_{21} & r'_{22} & r'_{23} \\ r_{31} & r'_{32} & r'_{33} \end{bmatrix}, \quad \phi_{MF} \equiv (\mathbf{j}_M, \mathbf{j}_F), \tag{13} $$

which leads to

$$ \mathbf{i}_F = \begin{bmatrix} r_{11} \\ r_{21} \\ r_{31} \end{bmatrix}, \quad \mathbf{j}_F = \begin{bmatrix} r'_{12} \\ r'_{22} \\ r'_{32} \end{bmatrix}, \quad \mathbf{k}_F = \begin{bmatrix} r'_{13} \\ r'_{23} \\ r'_{33} \end{bmatrix}. \tag{14} $$

Here, ϕ_{MF} is the angle between the two unit vectors $(\mathbf{j}_M, \mathbf{j}_F)$. Let the vector $\mathbf{P}$ be represented by ${}^F\mathbf{P}$ in the F-coordinate. Transformation of ${}^F\mathbf{P}$ into ${}^E\mathbf{P}$ contains rotation and translation,

$$ {}^E\mathbf{P} = {}^E_F\mathbf{R}(\psi_2,\psi_3,\phi_{MF}){}^F\mathbf{P} + \mathbf{X}. \tag{15} $$

Use of the F-coordinate system simplifies the calculations for the lift and drag forces and torques acting on the cylinder. Since the M and F-coordinates share a common axis $\mathbf{i}_M = \mathbf{i}_F$, the rotation matrix from the F to M-coordinate systems is given by

$$ {}^M_F\mathbf{R} = {}^M_E\mathbf{R}\,{}^E_F\mathbf{R} = {}^E_M\mathbf{R}^{-1}(\psi_2,\psi_3){}^E_F\mathbf{R}(\psi_2,\psi_3,\phi_{MF}) = \begin{bmatrix} 1 & 0 & 0 \\ 0 & e_{22} & e_{23} \\ 0 & e_{32} & e_{33} \end{bmatrix}, \tag{16} $$

is two-dimensional with the rotation matrix given by

$$ {}^M_F\mathbf{E} = [\mathbf{e}_2 \;\; \mathbf{e}_3], \quad \mathbf{e}_2 = \begin{bmatrix} e_{22} \\ e_{32} \end{bmatrix}, \quad \mathbf{e}_3 = \begin{bmatrix} e_{23} \\ e_{33} \end{bmatrix}. \tag{17} $$

Let the cylinder rotate around $(\mathbf{i}_F, \mathbf{j}_F, \mathbf{k}_F)$ with the angular velocity components represented by $(\omega'_1, \omega'_2, \omega'_3)$ (Fig. 2). They are connected to the angular velocity components in the M-coordinate system by

$$ \omega'_1 = \omega_1, \quad \begin{bmatrix} \omega'_2 \\ \omega'_3 \end{bmatrix} = {}^F_M\mathbf{E} \begin{bmatrix} \omega_2 \\ \omega_3 \end{bmatrix}. \tag{18} $$

3 Prediction of Hydrodynamic Characteristics of Falling Cylinder

3.1 Translation Velocity. The translation velocity of the cylinder ($\mathbf{V}$) is governed by the momentum equation in the E-coordinate system,

$$ \frac{d}{dt}\begin{bmatrix} u \\ v \\ w \end{bmatrix} = -\begin{bmatrix} 0 \\ 0 \\ (1-\rho_w/\overline{\rho})g \end{bmatrix} + \frac{1}{\overline{\rho}\Pi}\begin{bmatrix} F_x \\ F_y \\ F_z \end{bmatrix}, \tag{19} $$

where g is the gravitational acceleration; $\overline{\rho}$ is the average cylinder density; ρ_w is the water density; Π is the cylinder volume; and $\overline{\rho}\Pi = m$, is the cylinder mass; (F_x, F_y, F_z) are the hydrodynamic force (including drag and lift forces) components. The drag and lift forces are calculated using the drag and lift laws with the given water-to-cylinder velocity ($\mathbf{V}_r$) that is calculated using the F-coordinate.

3.2 Cylinder's Orientation. It is convenient to write the moment of momentum equation

$$ \mathbf{J}\cdot\frac{d\boldsymbol{\omega}}{dt} = \mathbf{M}_b + \mathbf{M}_h, \tag{20} $$

in the M-coordinate system with the cylinder's angular velocity components $(\omega_1, \omega_2, \omega_3)$ defined by (7). Here, $\mathbf{M}_b$ and $\mathbf{M}_h$ are the body and surface force torques. The moment of gyration tensor for the axially symmetric cylinder is a diagonal matrix

$$ \mathbf{J} = \begin{bmatrix} J_1 & 0 & 0 \\ 0 & J_2 & 0 \\ 0 & 0 & J_3 \end{bmatrix}, \tag{21} $$

where J_1, J_2, and J_3 are the moments of inertia. The gravity force, passing the COM, doesn't induce the moment. The buoyancy force induces the moment in the $\mathbf{j}_M$ direction if the COM doesn't coincide with the COV (i.e., $\chi \neq 0$),

$$ \mathbf{M}_b = \Pi\chi\rho_w g\cos\psi_2\mathbf{j}_M. \tag{22} $$

The moment of the hydrodynamic force in $\mathbf{i}_F$ direction is not caused by the drag and lift forces, but by the viscous fluid. The moment of the viscous force is calculated by (White [1])

$$ \mathbf{M}_{v1} = -C_{m1}\omega_1\mathbf{i}_F, \quad C_{m1} \equiv \pi\mu L d^2. \tag{23} $$

When the cylinder rotates around $\mathbf{j}_F$ with the angular velocity ω'_2, the drag force exerts the torque on the cylinder in the $\mathbf{j}_F$ direction ($\mathbf{M}_{d2}$) and in the $\mathbf{k}_F$ direction ($\mathbf{M}_{d3}$). The lift force exerts the torque on the cylinder in the $\mathbf{j}_F$ direction ($\mathbf{M}_{l2}$). The moment of hydrodynamic force $\mathbf{M}_h$

$$ \mathbf{M}_h = \mathbf{M}_{v1} + \mathbf{M}_{d2} + \mathbf{M}_{d3} + \mathbf{M}_{l2} \tag{24} $$

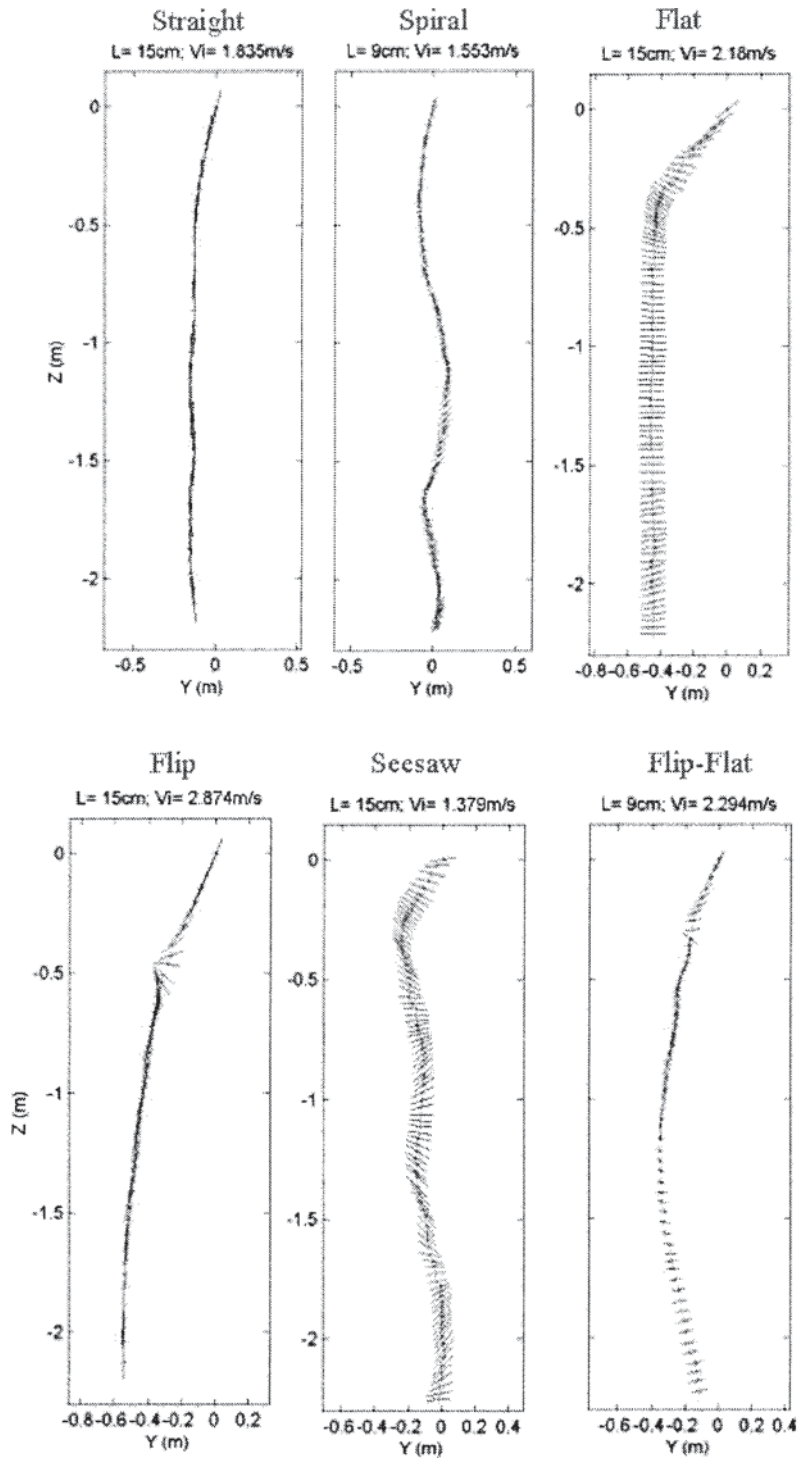

Fig. 3 Cylinders' track patterns observed during CYDEX

is represented in M-coordinate. Note that the M and F-coordinate systems have the same x-axis, $\mathbf{i}_M = \mathbf{i}_F$. The equations for $(\omega_1, \omega_2, \omega_3)$ are given by

$$\frac{d\omega_1}{dt} = -a_1\omega_1, \tag{25}$$

$$\frac{d}{dt}\begin{bmatrix}\omega_2\\ \omega_3\end{bmatrix} = -\mathbf{B}\cdot\begin{bmatrix}\omega_2\\ \omega_3\end{bmatrix} + \boldsymbol{\alpha}_2, \tag{26}$$

where

$$a_1 \equiv \frac{C_{m1}}{J_1} = 8\pi\mu L/m,$$

$$\mathbf{B} \equiv \begin{bmatrix}\frac{1}{J_2} & 0\\ 0 & \frac{1}{J_3}\end{bmatrix}\cdot\left(C_{m2}\mathbf{e}_2\mathbf{e}_2^T + C_{m3}\mathbf{e}_3\mathbf{e}_3^T - C_{ml}\mathbf{e}_2\mathbf{e}_3^T\right), \tag{27}$$

Table 3 Trajectory patterns for nose-down dropping ($\chi>0$)

Cylinder Length (cm) χ (cm)	15.20 1.48	12.10 1.00	9.12 0.58
Drop angle 15 deg	Straight (1) Slant-straight* (3)	Straight (1), Spiral (1) Slant-straight* (2)	Spiral* (2) Straight-slant (1) Slant-straight (1)
Drop angle 30 deg	Straight (1) Slant-straight* (4)	Slant (1), Spiral (1) Straight (1) Slant-straight* (2)	Spiral* (5)
Drop angle 45 deg	Slant* (2), Straight (1) Slant-straight (1) Straight-spiral (1)	Straight (1) Spiral* (2) Straight-spiral (1) Slant-straight (1)	Spiral* (4) Slant-spiral (1)
Drop angle 60 deg	Straight** (5)	Straight* (3) Straight-spiral (1) Straight-slant (1)	Spiral* (4) Straight-spiral (1)
Drop angle 75 deg	Straight** (5)	Straight (2) Straight-spiral (3)	Spiral (2), Slant (1) Straight-spiral (2)

$$\boldsymbol{\alpha}_2 \equiv \begin{bmatrix} \frac{1}{J_2} & 0 \\ 0 & \frac{1}{J_3} \end{bmatrix} \cdot (M_1 \mathbf{e}_2 - M_3 \mathbf{e}_3) + \frac{\Pi \chi g \rho_w}{J_2} \cos \psi_2 \begin{bmatrix} 1 \\ 0 \end{bmatrix}.$$

Here, $M_l \equiv 1/2 d\rho_w/(1+f_r)LV_2^2\chi$, $M_3 \equiv 1/2 C_{d2} d\rho_w/(1+f_r)V_2^2 L\chi$, and f_r is the added mass factor for the moment of drag and lift forces. Equation (25) has the analytical solution

$$\omega_1(t) = \omega_1(t_0)\exp[-a_1(t-t_0)], \tag{28}$$

which represents damping rotation of the cylinder around the main axis ($\mathbf{i}_M$). The Euler-typed forward difference is used to solve the five Eqs. (19), (26), and (28).

4 Model Evaluation

The Cylinder Drop Experiment (CYDEX) was conducted at the Naval Postgraduate School (NPS) in July 2001 (Chu et al. [2]) to evaluate the three-dimensional theoretical model. It consisted of dropping cylinders whose physical conditions are illustrated in Table 1 into the water and recording the position as a function of time using two digital cameras at (30 Hz) as the cylinders fell 2.4 meters to the pool bottom. After analyzing the CODEX experimental data, seven general trajectory patterns (Table 2) are identified: straight, slant, spiral, flip, flat, see-saw, and combination (Fig. 3). Dependence of the trajectory patterns on the cylinders' physical parameters and release conditions are illustrated in Table 3. The theoretical model predicts the motion of cylinder inside

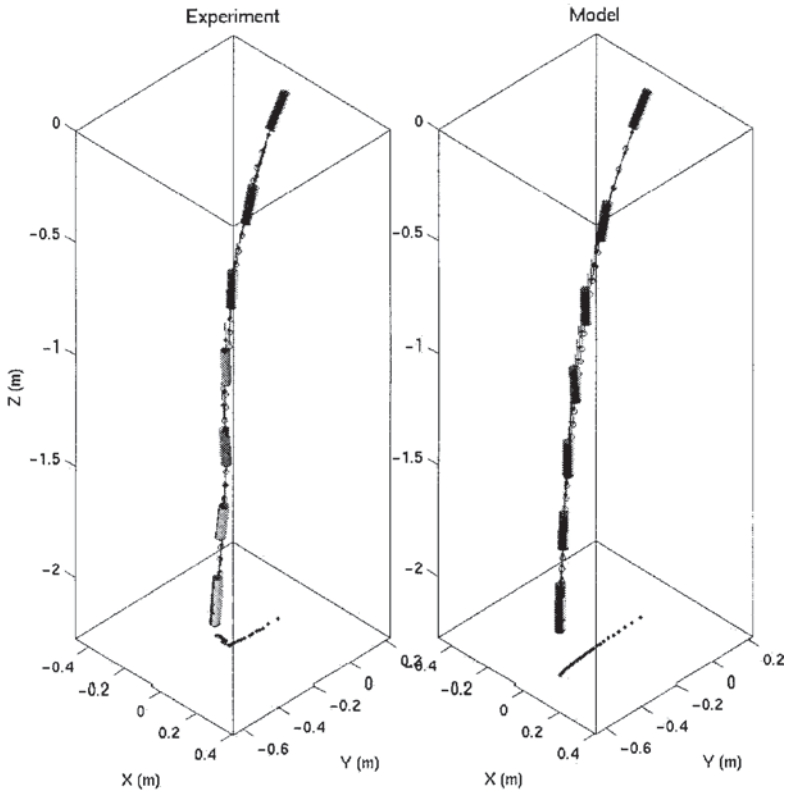

Fig. 4 Movement of Cylinder #1 ($L=15.20$ cm, $\bar{\rho}=1.69$ g cm^{-3}) with $\chi=0.74$ cm and drop angle 45 deg obtained from (*a*) experiment, and (*b*) recursive model

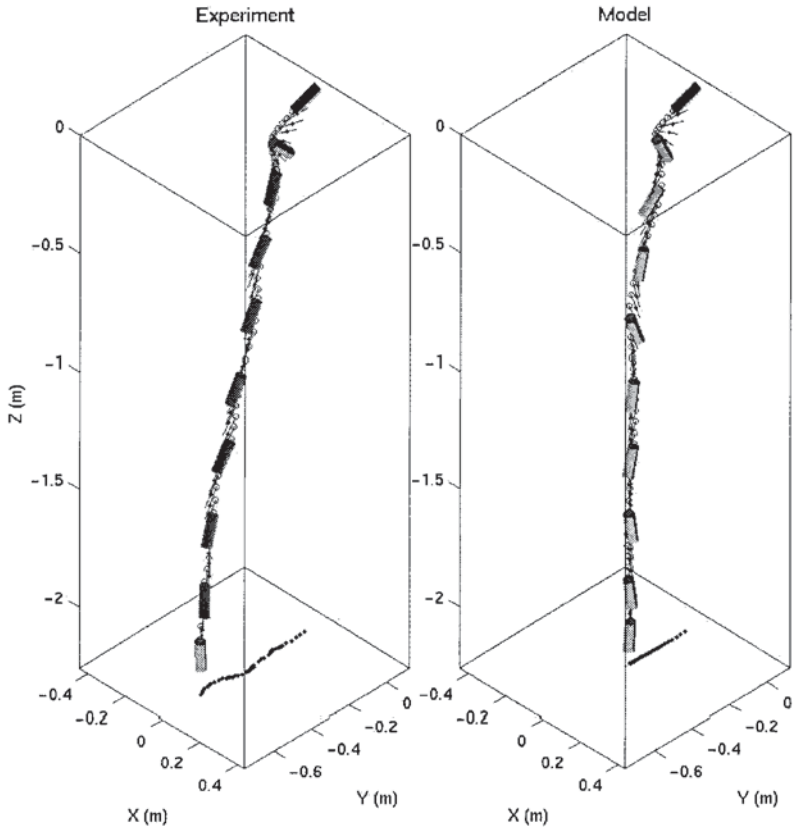

Fig. 5 Movement of Cylinder #2 ($L=12.10$ cm, $\bar{\rho}=1.67$ g cm^{-3}) with $\chi=-1.00$ cm and drop angle 30 deg obtained from (*a*) experiment, and (*b*) recursive model

the water column reasonably well. Two examples are listed for illustration.

Positive χ (Nose-Down). Cylinder #1 ($L=15.20$ cm, $\bar{\rho}=1.69$ g cm^{-3}) with $\chi=0.74$ m is injected to the water with the drop angle 45 deg. The physical parameters of this cylinder are given by

$$m=322.5 \text{ g}, \quad J_1=330.5 \text{ g cm}^2, \quad J_2=J_3=5783.0 \text{ g cm}^2. \tag{29a}$$

Undersea cameras measure the initial conditions

$$\begin{gathered} x_0=0, \quad y_0=0, \quad z_0=0, \quad u_0=0, \quad v_0=-1.55 \text{ m s}^{-1}, \\ w_0=-2.52 \text{ m s}^{-1}, \\ \psi_{10}=0, \quad \psi_{20}=60 \text{ deg}, \quad \psi_{30}=-95 \text{ deg}, \quad \omega_{10}=0, \\ \omega_{20}=0.49 \text{ s}^{-1}, \quad \omega_{30}=0.29 \text{ s}^{-1}. \end{gathered} \tag{29b}$$

Substitution of the model parameters (29*a*) and the initial conditions (29*b*) into the theoretical model ((19), (26), (28)) leads to the prediction of the cylinder's translation and orientation that are compared with the data collected during CYDEX at time steps (Fig. 4). Both model simulated and observed tracks show a slant-straight pattern.

Negative χ (Nose-Up): Cylinder #2 ($L=12.10$ cm, $\bar{\rho}=1.67$ g cm^{-3}) with $\chi=-1.00$ cm is injected to the water with the drop angle 30 deg. The physical parameters of this cylinder are given by

$$m=254.2 \text{ g}, \quad J_1=271.3 \text{ g cm}^2, \quad J_2=J_3=3312.6 \text{ g cm}^2. \tag{30a}$$

Undersea cameras measure the initial conditions

$$\begin{gathered} x_0=0, \quad y_0=0, \quad z_0=0, \quad u_0=0, \quad v_0=-0.75 \text{ m s}^{-1}, \\ w_0=-0.67 \text{ m s}^{-1}, \\ \psi_{10}=0, \quad \psi_{20}=24 \text{ deg}, \quad \psi_{30}=-96 \text{ deg}, \quad \omega_{10}=0, \\ \omega_{20}=-5.08 \text{ s}^{-1}, \quad \omega_{30}=0.15 \text{ s}^{-1}. \end{gathered} \tag{30b}$$

The predicted cylinder's translation and orientation are compared with the data collected during CYDEX at time steps (Fig. 5). The simulated and observed tracks show flip-spiral pattern. The flip occurs at 0.11 s (0.13 s) after cylinder entering the water in the experiment (model). After the flip, the cylinder spirals down to the bottom.

5 Conclusions

(1) Triple coordinate systems are suggested to predict the translation and orientation of falling rigid cylinder through water column: earth-fixed coordinate (E-coordinate), cylinder's main-axis following coordinate (M-coordinate), and hydrodynamic force following coordinate (F-coordinate). It simplifies the computation with the body and buoyancy forces and their moments in the E-coordinate system, the hydrodynamic forces (such as the drag and lift forces) and their moments in the F-coordinate, and the cylinder's moments of gyration in the M-coordinate.

(2) Usually, the momentum (moment of momentum) equation for predicting the cylinder's translation velocity (orientation) is represented in the E-coordinate (M-coordinate) system. Transformations among the three coordinate systems are used to convert the forcing terms into E-coordinate (M-coordinate) for the mo-

mentum (moment of momentum) equation. A numerical model is developed on the base of the triple coordinate transform to predict the cylinder's translation and orientation.

(3) Model-experiment comparison shows that the model well predicts the cylinder's translation and orientation. However, the performance of the numerical model for $\chi=0$ is not as good as for $\chi\neq 0$.

Acknowledgments

This research was funded by the Office of Naval Research Coastal Geosciences Program (grant N0001403WR20178), the Naval Oceanographic Office, and the Naval Postgraduate School supported this study.

References

[1] White, F. M., 1974, *Viscous Fluid Flow*, 1st Ed., McGraw-Hill, New York.

[2] Chu, P. C., Gilless, A. F., Fan, C., and Fleischer, P., 2002, "Hydrodynamical Characteristics of a Falling Cylinder in the Water Column," *Advances in Fluid Mechanics*, **4**, M. Rahman, R. Verhoeven, and C. A. Brebbia, eds., WIT Press, Southampton, UK, pp. 163–181.

Determination of Loads in an Inextensible Network According to Geometry of Its Wrinkles

Cheng Luo

Biomedical Engineering and Institute for Micromanufacturing, Louisiana Tech University, 911 Hergot Avenue, Ruston, LA 71272

e-mail: chengluo@latech.edu

This note derives an analytical relationship for an inextensible network when it buckles. According to the relationship, the applied compressive force can be determined according to the maximum absolute values of deflection and angle of deflection in the network's wrinkles. [DOI: 10.1115/1.1651094]

1 Introduction

If we pull both ends of a thin plastic sheet used for food packaging, a set of wrinkles, parallel to the loading direction, appears. Cerda and Mahadevan [1] and Cerda et al. [2] showed that the wavelength of the wrinkles is proportional to the square root of the sample size, and the tension can be determined according to the wavelength of the wrinkles. Fabric, such as cloth, is usually composed of two families of inextensible elastic fibers. The Poisson effect in the fabric may be different from that in the plastic sheet. For example, if the two families of fibers are loosely connected, then the Poisson effect may be neglected, while this cannot be true for the plastic sheet. Therefore, the modeling of an inextensible network may be different from that of a plastic sheet. In this note, we demonstrate that the applied compressive force on the fabric can be determined according to the maximum absolute values of deflection and angle of deflection in its wrinkles.

The effects of bending stiffness of a fiber network or an elastic surface have been well studied in the literature. Simmonds [3] considered elastic surfaces with resistance to strain and flexure, and Wang and Pipkin [4,5] studied inextensible nets with bending stiffness. Hilgers and Pipkin developed a theory of elastic sheets in a series of papers, [6–9], by introducing the second derivatives of the deformation as well as the first derivatives into the strain-energy density. Hilgers [10] also examined dynamic effects. Luo and Steigmann [11] established a model, a generalized plate/shell theory, to take into account the effects of bending and twisting in the inextensible networks for finite deformations in 3-space, and verified the soundness of a special form of finite-deformation plate theory developed by Wang and Pipkin in [4]. Wang and Pipkin [4] used their theory to consider the Euler buckling problem of a flat inextensible network, and indicated that the governing equation of the flat sheet during the buckling is identical to that for finite-amplitude oscillation of a simple pendulum. In this work, we further explore the buckling problem to determine the applied load on the inextensible network according to geometry of its wrinkles.

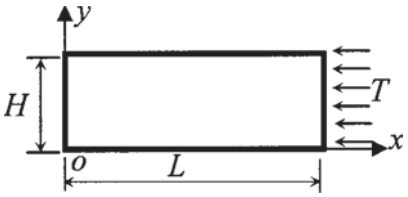

Fig. 1 Top view of the flat sheet before wrinkling

2 An Analytical Relationship

Consider a flat sheet that initially occupies the region $0<x<L$, $0<y<H$ in the x-y plane. The sheet is composed of two families of inextensible fibers, which initially lie parallel to the x and y-axes; thus every line $x=$constant or $y=$constant in the region is regarded as a fiber. The two families of fibers are orthogonal in the reference configuration. They are assumed to be continuously distributed and fastened together at their points of intersection to prevent slipping of one fiber family relative to the other. The sheet is treated as a continuum. Each fiber meets the Bernoulli-Euler hypotheses: cross sections of each fiber remain plane, suffer no strain, and are normal to the fiber in every configuration. A uniform force T per unit length is applied to the edge $x=L$ as a dead load along the negative direction of x-axis (see Fig. 1), and edges $y=0$ and $y=H$ are free from applied tractions and couples and displacement restrictions. The possible boundary conditions of physical meaning on the sides $x=0$ and $x=L$ can be classified into four categories: (i) both sides $x=0$ and $x=L$ are simply supported; (ii) the side $x=0$ is clamped and the side $x=L$ is free; (iii) both sides $x=0$ and $x=L$ are clamped; and (iv) the side $x=0$ is clamped and the side $x=L$ is simply supported. For any set of those boundary conditions, a solution is that the family of fibers with $x=$constant remain straight lines, the family of fibers with $y=$constant have identical deflections in the x-z plane and have no deflections in the other planes, and the two families of fibers are still orthogonal in the deformed configuration (see Fig. 2). Let $\theta(x)$ denote the angle between the tangent to the deflection curve and the x-y plane. Then it satisfies the equation, [4],

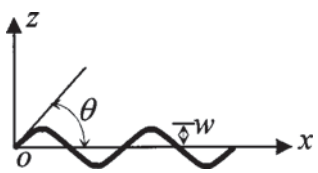

Fig. 2 Side view of a possible deformed configuration of the sheet

Contributed by the Applied Mechanics Division of THE AMERICAN SOCIETY OF MECHANICAL ENGINEERS for publication in the ASME JOURNAL OF APPLIED MECHANICS. Manuscript received by the ASME Applied Mechanics Division, June 2, 2003, final revision, September 19, 2003. Associate Editor: O. O'Reilly.